

Thermoelectric properties of the layered Pd oxide R_2PdO_4 ($R = La, Nd, Sm$ and Gd)

S. Shibasaki*

Department of Applied Physics, Waseda University, Tokyo 169-8555, Japan

I. Terasaki

*Department of Applied Physics, Waseda University, Tokyo 169-8555, Japan
also CREST, Japan Science and Technology Agency, Tokyo 108-0075, Japan*

We prepared polycrystalline samples of R_2PdO_4 ($R = La, Nd, Sm$ and Gd) using a NaCl-flux technique. The measured resistivity is of the order of 10^3 - 10^4 Ωcm at room temperature, which is two orders of magnitude smaller than the values reported so far. We further studied the substitution effects of Ce for Nd in $Nd_{1.9}Ce_{0.1}PdO_4$, where the substituted Ce decreases the resistivity and the magnitude of the thermopower. The activation energy gap of 70-80 meV and the effective mass of 15 evaluated from the measured data are suitable for thermoelectric materials, but the mobility of 10^{-6} cm^2/Vs is much lower than a typical value of 1-10 cm^2/Vs for other thermoelectric oxides.

PACS numbers:

I. INTRODUCTION

The thermoelectric properties of transition-metal oxides have attracted increasing attention year by year, since the good thermoelectric properties of the layered Co oxide Na_xCoO_2 were discovered [1]. Although the layered Co oxides are promising candidates for p-type thermoelectric materials, [2, 3] various n-type oxides, *e.g.*, $(Zn_{1-x}Al_x)O$, $(ZnO)_kIn_2O_3$, $Sr_{0.9}Dy_{0.1}TiO_3$, and $Sr_{0.9}Y_{0.1}TiO_3$ are not yet better than them. [4, 5, 6, 7] Thus a new n-type thermoelectric oxide is desired for all-oxide thermoelectric devices.

Recently, $Ca_{1-x}Li_xPd_3O_4$ turned out to be a good p-type thermoelectric material [8], and $Ca_{1-x}Bi_xPd_3O_4$ was found to be an n-type material [9]. $Ca_{1-x}Bi_xPd_3O_4$ is the first example of the n-type Pd oxide, and is interesting in the sense that electrons are doped in the $d_{x^2-y^2}$ band separated from the $d_{3z^2-r^2}$ band by a small energy gap of 0-10 meV. One serious drawback against good thermoelectrics was a small effective mass with a low mobility. [10] In addition, substitution of Bi for Ca cannot change the doping level so widely, because the solubility limit of Bi is at most 15 % that corresponds to only 5 % of electrons per Pd. Thus, we had to find another Pd oxide for n-type thermoelectric materials in which carrier concentration can be changed more widely.

Among various Pd oxides, we focused on R_2PdO_4 , ($R = La, Nd, Sm,$ and Gd) which is isomorphic to $Nd_{2-x}Ce_xCuO_4$, a famous n-type high-temperature superconductor [11]. The Pd^{2+} ion of $4d^8$ is surrounded with four planar oxygen atoms, in which the $d_{x^2-y^2}$ orbital is expected to be the lowest unoccupied state. Through substitution of Ce for R, we expect that electrons can be doped in the $d_{x^2-y^2}$ band, and let the sample be an n-type conductor. As is similar to the CuO_2 plane

in $Nd_{2-x}Ce_xCuO_4$, we expect that the PdO_2 plane would be metallic with a wide $pd\sigma^*$ band.

II. EXPERIMENT

Polycrystalline samples of R_2PdO_4 ($R = La, Nd, Sm$ and Gd) and $Nd_{1.9}Ce_{0.1}PdO_4$ were prepared by a solid-state reaction using a NaCl-flux technique [8]. Stoichiometric amounts of La_2O_3 , Nd_2O_3 , Sm_2O_3 , Gd_2O_3 , CeO_2 and PdO of 99.9 % purity were thoroughly mixed. NaCl was then added in a mass ratio of 2:1, thoroughly mixed again, and were fired at 1073 K for 24 h in air. The product was finely ground, and NaCl was rinsed out in hot distilled water. The powder was dried, palletized and sintered at 1073 K for 12 h in air. The low sintering temperature of 1073 K prevented cations from evaporating from the pellets, which was verified through the composition analyses of $Ca_{1-x}Li_xPd_3O_4$ previously. [8] We did not check the oxygen content, but as shown below, the magnitude of the thermopower of R_2PdO_4 is 200-600 $\mu\text{V}/\text{K}$ at 300 K, clearly indicating that they are almost undoped. This implies that the formal valence of Pd is close to 2+, and that the oxygen content is almost 4. Thus we refer the samples by nominal compositions in the present paper.

The black-colored samples were characterized by powder x-ray diffraction (XRD) using Cu $K\alpha$ radiation from $2\theta = 10$ to 100 deg. The resistivity was measured by a four-probe method, and the thermopower was measured by a steady method. The magnetization measurement was done with an SQUID susceptometer (Quantum Design MPMS) from 6 to 300 K in a field B_{ex} of 0.1 T.

III. RESULTS AND DISCUSSION

Figure 1(a) shows typical XRD patterns of the prepared samples, which are indexed as R_2PdO_4 with a small amount of unreacted PdO and CeO_2 . In previous

*Electronic address: g01k0374@suou.waseda.jp

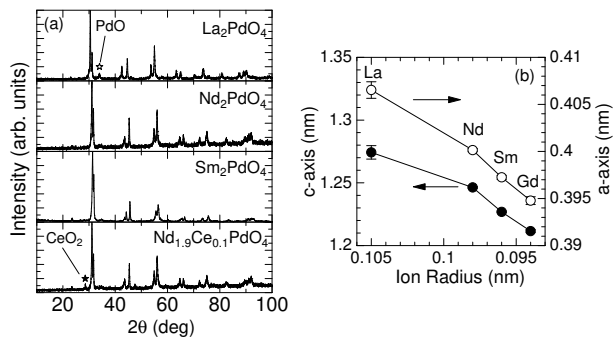


FIG. 1: (a) X-ray diffraction patterns of R_2PdO_4 ($R = La, Nd$ and Sm) and $Nd_{1.9}Ce_{0.1}PdO_4$, and (b) lattice constants of R_2PdO_4 ($R = La, Nd, Sm$ and Gd).

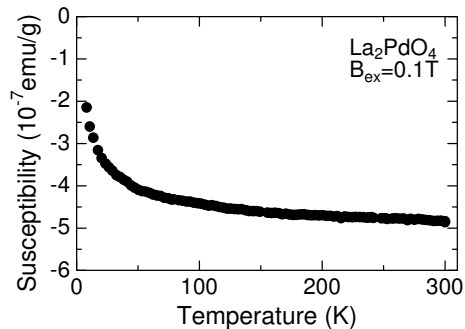


FIG. 2: The susceptibility of La_2PdO_4 in an external field B_{ex} of 0.1 T.

works [12, 13], polycrystalline samples of La_2PdO_4 included impurity phases like $La_2Pd_2O_5$ or La_4PdO_7 . Figure 1(a) shows no trace of such phases, which indicates that the NaCl-flux technique is very effective to stabilize La_2PdO_4 . Lattice constants evaluated from Fig. 1(a) are plotted as a function of ionic radius of R in Fig. 1(b), indicating that the a - and c -axis lengths systematically decrease with decreasing ion radius of R.

In order to check the magnetic state of the Pd ion, we measured the susceptibility of La_2PdO_4 . Note that Nd, Sm and Gd are magnetic ions with localized f electrons, which will obscure the susceptibility of the Pd ions. As shown in Fig. 2, the susceptibility of La_2PdO_4 is as small as that of a diamagnetic substance like water. This means that the susceptibility is determined by the diamagnetism of core electrons, and that Pd^{2+} is nonmagnetic. Thus we can safely assume that the Pd ions are in the low-spin state with the configuration of $(t_{2g})^6(d_{3z^2-r^2})^2(d_{x^2-y^2})^0$, and that the $d_{x^2-y^2}$ band is unoccupied, as expected in the introduction. Toward 0 K, the susceptibility slightly increases, possibly caused by a small amount of impurity phases. Fitting the data with the Curie-Weiss law, we evaluated a maximum volume fraction of the magnetic impurity to be 0.1 %.

Figure 3(a) shows the resistivity of the prepared sam-

ples. The magnitudes are 10^3 - 10^4 Ω cm at 300 K, and rapidly increases with decreasing temperature. These results indicate that R_2PdO_4 is an undoped insulator, which is consistent with the small diamagnetic susceptibility of La_2PdO_4 . We note that the resistivity of our samples at room temperature is two orders of magnitude smaller than the previously reported values [14]. This is consistent with the fact that our samples did not include impurity phases like $R_2Pd_2O_5$ and R_4PdO_7 .

Figure 3(b) shows that the thermopower of the prepared samples. All the samples show a negative sign, indicating that R_2PdO_4 is an n-type conductor. A similar negative thermopower is seen in the n-type copper oxide Nd_2CuO_4 that is isomorphic to the title compound. [11] The magnitude is as large as 200-600 μ V/K at 300 K, which indicates that the carriers are almost undoped. Considering that conventional thermoelectric materials show a thermopower of 200 μ V/K at 300 K, we conclude that the carrier density is somewhat lower than that of them. Comparing with a typical carrier density (10^{19} - 10^{20} cm^{-3}) of conventional thermoelectric materials, we estimate the carrier density of R_2PdO_4 to be of the order of 0.01 electrons per Pd ion.

One may notice that the magnitude of the thermopower systematically increases in going from $R = La$ to Gd, which suggests that the carrier density systematically decreases from La to Gd. Similarly, the resistivity is highest for Gd_2PdO_4 , and is lowest for Nd_2PdO_4 . (La_2PdO_4 shows higher resistivity than Sm_2PdO_4 . This does not follow the trend, possibly owing to poorer sintering. In fact, a larger amount of PdO is detected in La_2PdO_4 in Fig. 1.) Since the estimated carrier density is of the order of 1 % per Pd, a small cation deficiency of less than 1 % will significantly affect the transport parameters. The ionic radius of R systematically decreases with increasing atomic number, and the deficiency in the R site will possibly vary with the ionic radius. A similar example is seen in the parent insulator of high-temperature superconductor $Bi_2Sr_2Er_{1-x}Dy_xCu_2O_{8+\delta}$, in which the carrier density systematically decreases with increasing x . [15]

Let us analyze the resistivity and thermopower more quantitatively. As mentioned above, R_2PdO_4 is a nearly undoped semiconductor with an energy gap between the $d_{x^2-y^2}$ and $d_{3z^2-r^2}$ bands. Thus we expect a conventional semiconductor physics that the transport properties at high temperatures are of activation type characterized by the band gap, and those at low temperatures are of variable-range-hopping (VRH) type. The crossover will occur when the thermally activated carriers are comparable to the doped carriers in number. That is, the more carriers are doped, the higher the crossover temperature is. Accordingly, we expect that the activation-type conduction is realized below 300 K for the least doped sample Gd_2PdO_4 .

The activation-type resistivity and thermopower are

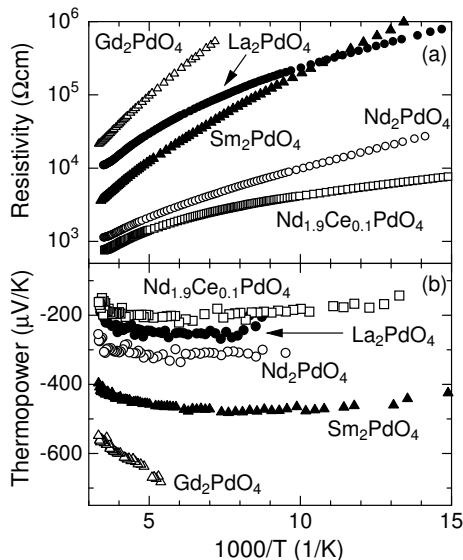


FIG. 3: (a) Resistivity and (b) thermopower of $R_2\text{PdO}_4$ ($R = \text{La, Nd, Sm and Gd}$) and $\text{Nd}_{1.9}\text{Ce}_{0.1}\text{PdO}_4$.

written by

$$\rho \propto \exp\left[\frac{E_g}{k_B T}\right], \quad (1)$$

$$S \propto \left[\frac{E_s}{eT} + \text{const.}\right]. \quad (2)$$

Then the resistivity plotted in a log scale and the thermopower plotted in a linear scale are inversely proportional to temperature. As shown in Fig. 3, the data for Gd_2PdO_4 roughly obey these relations. The activation energies are evaluated to be $E_g=80.7$ meV from the resistivity and $E_s=73.6$ meV from the thermopower. A relation of $E_g \sim E_s$ strongly suggests that the activation process in Gd_2PdO_4 is determined by carrier density thermally excited across the band gap. In other words, $E_g \sim E_s$ is the energy gap between the $d_{x^2-y^2}$ and $d_{3z^2-r^2}$ bands. Since these two bands would be degenerate in the cubic symmetry, the small band gap less than 100 meV evaluated here is reasonable.

We should note here that the relation of $E_g \gg E_s$ is often seen in $3d$ transition-metal oxides, where the carriers distort the lattice nearby through the strong electron-phonon interaction to be stabilized in the potential well of the distorted lattice.[16] This “self-trapped” state is called a (small) polaron, and such a material is called a polaronic conductor. We expect an activation-type conduction in polaronic conductors, where the activation energy comes from the potential well (the polaron binding energy), not from the band gap. This means that the mobility or the scattering time obeys the activation law. Since the thermopower is independent of the scattering time in the lowest order approximation, [17] $E_g \gg E_s$ is expected in a polaron semiconductor, where E_s is the band gap and $E_g - E_s$ is the polaron binding energy.[18]

In this context, the relation $E_g \sim E_s$ in Gd_2PdO_4 is rather unusual in the transition-metal oxides, which implies that a band picture works well to some extent in the $4d$ transition-metal oxides, possibly owing to the broader $4d$ bands than the $3d$ bands.[19]

The other three samples (La_2PdO_4 , Nd_2PdO_4 and Sm_2PdO_4) are more doped than Gd_2PdO_4 , and show the VRH-type transport expressed by

$$\rho \propto \exp\left[\left(\frac{T_0}{T}\right)^{\frac{1}{d+1}}\right], \quad (3)$$

where d is the dimension of the system [20]. The data are fitted well with $d = 2$ or $d = 3$, as shown in Fig. 4. The characteristic temperature T_0 is a measure of the localization length ξ through $T_0 \propto 1/k_B D \xi^d$, where D is the density of states at the Fermi energy. Figure 4 shows that T_0 is roughly the same among $R = \text{La, Nd and Sm}$. Since D does not change very much with R , the localization length ξ is roughly the same in $R_2\text{PdO}_4$.

The thermopower of the three samples shows a broad maximum around 100-200 K in Fig. 3(b), which is consistent with the VRH picture of a slightly doped semiconductor. The VRH-type thermopower is given by [21]

$$S \propto T^{\frac{d-1}{d+1}}. \quad (4)$$

Accordingly, the sublinear thermopower ($S \propto T^{1/3}$ for $d = 2$ or $S \propto T^{1/2}$ for $d = 3$) is expected at low temperatures, and the activation-type thermopower of Eq. (2) is expected at high temperatures. The broad maximum observed around 100-200 K is a sign for the crossover between the two regimes. The sublinear thermopower should have been observed below 100 K, but the sample resistance was too high to measure reliable thermoelectric voltage below 100 K in our experimental setup.

The thermoelectric performance is characterized by the power factor (S^2/ρ), which is a measure of the maximum electric power generated from thermal energy.[10] Figure 3 shows that S^2/ρ at 300 K takes the maximum for $R = \text{Nd}$. Thus we partially substituted Ce for Nd in Nd_2PdO_4 to see the doping effects. Although a tiny peak of CeO_2 is present in $x=0.1$ in Fig. 1(a), the resistivity and thermopower decrease from those for Nd_2PdO_4 , as shown in Fig. 3. This suggests that a substantial portion of Ce is substituted for Nd to supply holes, and further suggests that $\text{Nd}_{1.9}\text{Ce}_{0.1}\text{PdO}_4$ is a metal (or a degenerate semiconductor) with a finite Fermi energy E_F in the low temperature limit ($T \rightarrow 0$). Then the thermopower at low temperatures is given by [17]

$$S = -\frac{\pi^2 k_B^2 T}{2e E_F}. \quad (5)$$

On the other hand, in the high temperature limit of $E_F \ll k_B T$, the thermopower becomes temperature-independent, and obeys the Heikes formula given by[22]

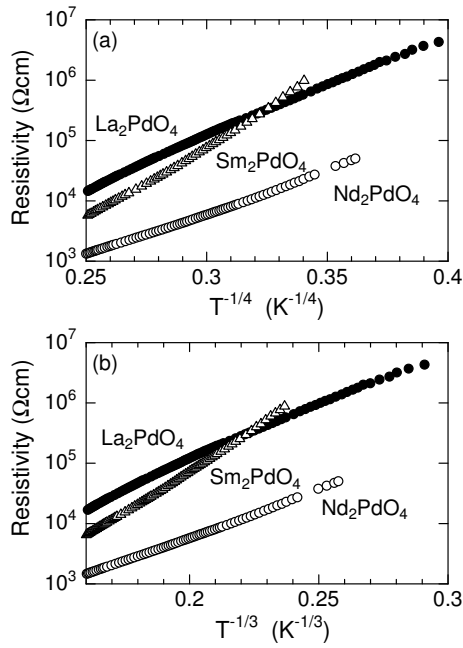


FIG. 4: Resistivity for R_2PdO_4 ($R = La, Nd$ and Sm) plotted as a function of (a) $T^{-1/4}$ and (b) $T^{-1/3}$.

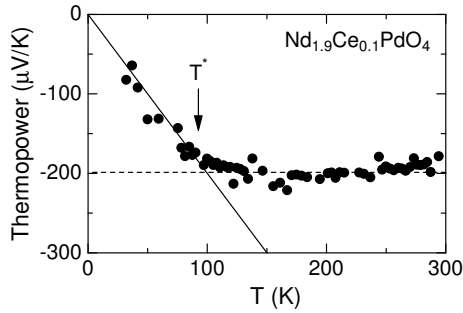


FIG. 5: Thermopower of $Nd_{1.9}Ce_{0.1}PdO_4$. The solid and dotted lines represent Eqs. (5) and (6), respectively. The crossover temperature T^* is indicated by an arrow.

$$S = -\frac{k_B}{e} \ln \left| \frac{2(1-N)}{N} \right|, \quad (6)$$

where N is the number of carriers per Pd.

As shown by the solid and dotted lines in Fig. 5, the fitting with Eqs. (5) and (6) are satisfactory. E_F is evaluated to be 16.5 meV from Eq. (5), corresponding to a thermal energy of 200 K that is close to the crossover temperature $T^* \sim 100$ K. Substituting the saturated value of $S = -200 \mu V/K$ into Eq. (6), we get the carrier density $n = 1.6 \times 10^{21} \text{ cm}^{-3}$, which is of the same order of the ideal value that each Ce ion supplies one electron. Combining with n and E_F , we evaluate the effective mass m^* to be 15 through the following equation

$$E_F = \hbar^2 \pi d_c \frac{n}{m^*}, \quad (7)$$

where d_c is the interlayer distance [23]. The heavy m^* and the small E_g are favorable to good thermoelectrics [10], but the mobility μ evaluated from $\mu = 1/nep$ is of the order of $10^{-6} \text{ cm}^2/Vs$ at 300 K which is much smaller than a typical mobility of thermoelectric oxides ($1-10 \text{ cm}^2/Vs$ at 300 K).

IV. SUMMARY

We prepared polycrystalline samples of R_2PdO_4 ($R = La, Nd, Sm$ and Gd) and $Nd_{1.9}Ce_{0.1}PdO_4$ using NaCl flux. They are n-type materials with the thermopower of $-600 \sim -200 \mu V/K$ at room temperature. The resistivity of R_2PdO_4 is semiconductive, characterized by an activation energy of 70-80 meV. By the Ce substitution, electrons are doped to reduce the resistivity and thermopower in magnitude. From the thermopower, the carrier concentration and the effective mass are evaluated to be $1.6 \times 10^{21} \text{ cm}^{-3}$ and 15, respectively. The mobility is poor, which might be improved through different synthetic routes.

Acknowledgments

We thank W. Kobayashi, S. Okada and S. Ishiwata for useful comments.

-
- [1] I. Terasaki, Y. Sasago and K. Uchinokura: Phys. Rev. **B56**(1997) R12685.
 - [2] R. Funahashi, I. Matsubara, H. Ikuta, T. Takeuchi, U. Mizutani and S. Sodeoka: Jpn. J. Appl. Phys. **39**(2000) L1127.
 - [3] R. Funahashi and I. Matsubara: Appl. Phys. Lett. **79**(2001) 362.
 - [4] M. Ohtaki, T. Tsubota, K. Eguchi, and H. Arai: J. Appl. Phys. **79**(1996) 1816.
 - [5] H. Hiramatsu, W. S. Seo and K. Koumoto: Chem. Mater. **10**(1998) 3033.
 - [6] H. Muta, K. Kurosaki and S. Yamanaka: J. Alloy. Comp. **350**(2003) 292.
 - [7] H. Obara, A. Yamamoto, C. H. Lee, K. Kobayashi, A. Matsumoto and R. Funahashi: Jpn. J. Appl. Phys. **43**(2004) L540.
 - [8] S. Ichikawa and I. Terasaki: Phys. Rev. **B68**(2003) 233101.

- [9] S. Ichikawa, S. Shibusaki and I. Terasaki: *Proc. 23rd Int. Conference on Thermoelectrics*, (ICT2004), IEEE, Piscataway (in press).
- [10] G. D. Mahan: *Solid State Phys.* **51**(1998) 81.
- [11] Y. Tokura, H. Takagi and S. Uchida: *Nature* **337**(1989) 345.
- [12] B. G. Kakhan, V. B. Lazarev and I. S. Shaplygin: *Russ. J. Inorg. Chem.* **27**(1982) 1182.
- [13] J. P. Attfield and G. Férey: *J. Solid State Chem.* **80**(1989) 286.
- [14] B. G. Kakhan, V. B. Lazarev and I. S. Shaplygin: *Russ. J. Inorg. Chem.* **27**(1982) 1352.
- [15] T. Takayanagi, M. Kogure and I. Terasaki: *J. Phys. Condens. Matter* **14** (2002) 1361.
- [16] W. Kobayashi, A. Satake and I. Terasaki: *Jpn. J. Appl. Phys.* **41**(2002) 3025.
- [17] N. W. Ashcroft and N. D. Mermin: *Solid State Physics* (Saunders College Publishing, Philadelphia, 1975).
- [18] T. T. M. Palstra, A. P. Ramirez, S-W. Cheong, B. R. Zegarski, P. Schiffer, and J. Zaanen: *Phys. Rev. B* **56** (1997) 5104.
- [19] I. Terasaki: *Proc. 24th Int. Conference on Thermoelectrics* (ICT2005), Clemson, June 19-23, 2005 (in press).
- [20] N. F. Mott and E. A. Davis: *Electronic processes in non-crystalline materials* (Clarendon press, New York, 1979).
- [21] M. J. Burns and P. M. Chaikin: *Phys. Rev.* **B27**(1983) 5924.
- [22] P. M. Chaikin and G. Beni: *Phys. Rev.* **B13**(1976) 647.
- [23] V. Z. Kresin and S. A. Wolf: *Phys. Rev.* **B41**(1990) 4278.